CFD-Based Optimization and Performance Analysis of a Solar Still Using Geometrical Parameters

Mayank Paswan[1], Sanjay Kumar Singh[2], Shivshankar V. Choudri[3]
[1] Research scholar,Department of Mechanical engineering, SISTECH BHOPAL (M.P.)
[2] Professor,Department of Mechanical engineering, SISTECH BHOPAL (M.P.)
[3] HOD,Department of Mechanical engineering, SISTECH BHOPAL (M.P.)
[1] Mrigankp299@gmail.com, [2]sanjaysingh@sistec.ac.in, [3]sistec.hodme@sistec.ac.in

* Corresponding Author: Mayank Paswan

Abstract: *This research focuses on optimizing solar stills to improve potable water production, responding to the critical global need for clean drinking water. The study aimed to enhance productivity by varying geometrical parameters, optimizing mass flow, and comparing conventional designs with new proposals. ANSYS simulations were utilized to evaluate both single and double sloped solar stills, revealing significant improvements in water yield through turbulence-enhancing techniques, with ultrasonic fogging showing up to an 83.87% increase in productivity. Structural optimizations, including adjustments to weir height and component distances, achieved a maximum water production rate of 6.474 kg/m² day. These findings highlight the effectiveness of design modifications and turbulence methods in increasing solar still efficiency, providing practical solutions for addressing water scarcity.*

Keywords:*Solar stills, potable water production, ANSYS simulations, turbulence methods, ultrasonic fogging, geometrical optimization, mass flow, inclined solar stills, water scarcity, solar distillation efficiency*.

I. Introduction

There is an urgent need for clean, pure drinking water in many countries. Often, water sources are brackish and/or containing harmful bacteria and therefore cannot be used for drinking. In addition, there are many coastal locations where sea water is abundant but potable water is not available. Pure water is also needed in some industries, hospitals and schools. Solar distillation is one of many processes that can be used for water purification. Solar radiation can be the source of heat energy where brackish or sea water is evaporated and is then condensed as pure water [1]. In the last forty years the problem of clean drinking water is one of the challenges facing the world. Clean drinking water is a basic human necessity, and without water life will be impossible. In addition, with an ever-increasing population and rapid growth of industrialization, there is a great demand for fresh water, especially for drinking. One of the options used to obtain pure drinking water from saltwater is to use solar desalination plants. Solar stills represent a good option and a simple technique compared to the other distillation methods. The problem facing the solar stills is the low distillate water productivity. To enhance the productivity of the solar still, various research works are being carried out [2]. The potable water demand worldwide is increasing due to the increase in population and life modernization, while most of the available water cannot be used for drinking due to salinity and/or water contamination. These types of waters could be utilized for drinking and for use in some industries after removal of salts and harmful contaminants. There are numerous methods used for water purification including filtration, disinfection, sedimentation and distillation. Solar distillation is one of the most important water purification processes. The main idea of solar distillation is to use solar radiation as a source of heat to evaporate brackish water, then condense the vapor on a surface and collect the condensed water as pure water. Solar still is a device used in solar distillation process to produce potable water. This device is a cheap unit and can be designed from abundant and cheap materials. The basic idea of a solar still is that salty or dirty water in an airtight container is heated by solar energy, causing it to evaporate. Water vapor then condenses on an inclined glass covering surface, in order to allow fresh water to drain into a collection unit. Pure water evaporates and the impurities do not, distilling water and making it safe to drink [3].

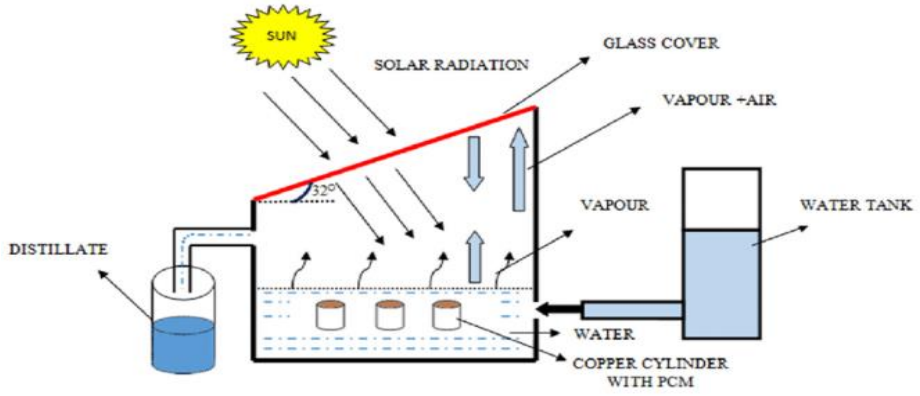

Figure 1 Schematic diagram of passive solar still with PCM [4]

The thermal energy can also be stored in the phase change material (PCM). It was noted that the PCMs store larger amount of heat compared to the sensible heat storage materials because the PCMs have high energy storage capacity per unit volume and almost constant temperature for charging and discharging [43]. The main disadvantage of using PCMs is the leakage problem when it is in the liquid phase. There is one important condition when using a PCM as a heat storage material integrated with the solar stills; it is desirable that the maximum temperature of the basin water should around the melting point of the PCM [5].

A. Types of Solar Stills

Solar stills can be sub divided in to two kinds:

i. **Passive Solar Stills:** Still solar systems that use solar energy as their primary source of heat energy and those that are combined with solar thermal energy are directly used to heat water and then produce the distillation effect. The low operating temperature and vapor pressure explain this development rate [6].

ii. **Active Solar Stills:** Extra thermal energy of this form is combined with passive solar for faster evaporation and this extra thermal energy can be collected from a solar collector or any excess thermal energy generated from any industrial plant.[6]

B. Phase Change Materials (PCM)

Solid-liquid Phase Change Materials (PCMs) have been explored extensively for their role in thermal management and energy storage, thanks to their significant latent heat capacity and minimal temperature or volume change. Advances in electrification, including photovoltaics, wind energy, high-power electronic devices, and electrified transportation, have renewed interest in using PCM for thermal storage. PCMs are beneficial for managing transient heat loads, balancing renewable energy generation with demand, storing large-scale energy, recovering waste heat, and supporting carbon neutrality efforts. They offer a cost-effective and easily integrable solution compared to other storage methods like electrochemical batteries, especially when paired with readily available energy sources such as solar power [7]. The Thermal Energy Storage (TES) method also improves the performance of many devices in various industries. Phase change materials (PCM) are excellent materials for storing thermal energy. PCMs are Latent Heat Storage Materials (LHS) that absorb and release large amounts of heat during changing the phase changes from solid to liquid or liquid to solid [8]. The performance of TES and heat transfer depends on the thermal conductivity of the substance.

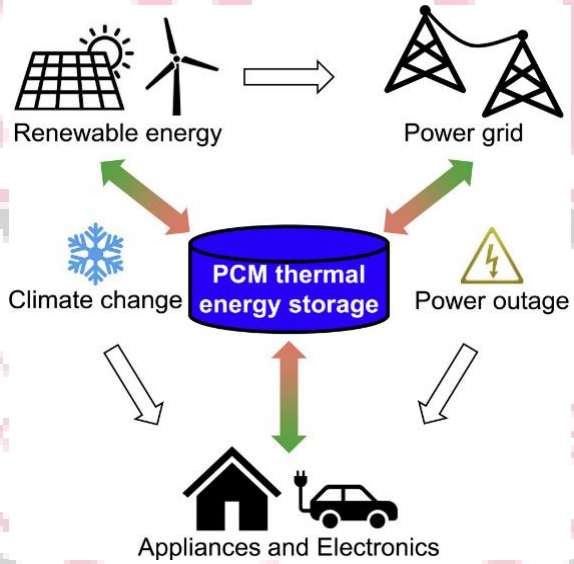

Figure 2 PCM Thermal Energy Storage in Renewable Energy Systems

C. Significance

Solar desalination is one of the most important renewable energy-powered techniques for producing freshwater. It has become increasingly popular due to its availability in geographically remote areas, low cost of energy utilization, and environmental friendliness. Solar desalination methods include Multiple-Effect Humidification (MEH), Multi-Stage Flash Distillation (MSF), Multiple-Effect Distillation (MED), Multiple-Effect Boiling (MEB), Humidification–Dehumidification (HDH), and solar stills. Solar stills offer several advantages, such as simple and low-cost design and environmental friendliness [9]. Solar energy, harnessed for distillation, has proven to be an effective and non-conventional approach. Researchers worldwide have developed, fabricated, and tested various designs of solar distillation systems, encompassing both passive and active methods. The findings of these studies have been meticulously documented, serving as valuable insights for scientists in this field. Passive solar distillation, mirroring the natural processes of evaporation and condensation, has undergone comprehensive analysis to enhance our understanding of its efficacy [10].

D. Applications

i. **Desalination:** Desalination based on vapor generation from saltwater powered by solar energy has emerged as one of the most promising methods for clean water harvesting among several desalination technologies. Adsorption desalination is a promising technology that uses biomass or solar energy as a low-temperature heat source to provide drinkable water. It is a desalination technique that uses less energy. Reverse osmosis, multi-effect distillation, and multi-stage flash are conventional desalination techniques that use much energy. The adsorption desalination technology is a useful alternative to these traditional techniques. Adsorption desalination/cooling systems are an alternative technology powered by renewable energy at low temperatures [11].

ii. **Rural Water Supply:** In rural and arid regions where conventional water infrastructure is often sparse or non-existent, solar stills equipped with phase change materials (PCMs) offer a practical and sustainable solution for water supply. These systems harness solar energy to distill seawater or brackish water, leveraging the PCM's ability to store and release thermal energy efficiently. By operating effectively even during periods of limited sunlight, such as cloudy days or nighttime, these solar stills can continuously produce clean, fresh water. This capability is crucial for improving water access in underserved areas, supporting local communities, and promoting self-sufficiency in regions where traditional water resources are either insufficient or inaccessible [12].

iii. **Solar Water Heating:** In solar water heating systems, the integration of phase change materials (PCMs) allows for the effective storage of excess heat generated during sunny periods. By capturing and retaining this thermal energy, the system can release it gradually, ensuring that hot water remains available even during nighttime or cloudy conditions. In doing so, the system enhances the reliability of hot water supply and boosts overall efficiency. This reduces the need for additional heating sources and lowers energy costs, providing a more consistent and sustainable solution for domestic hot water needs while contributing to energy conservation and cost savings [13].

II. Literature Review

Abdullah, A. et al. (2023) [14] explained that everyday living, the need for fresh water is crucial. The most pressing problem in developing nations is the ongoing lack of access to clean water. In many ways, the solar still is a great source of freshwater for both drinking and cultivation, it is one of the most popular essential and technically practicable sun energy uses. This study lists studies on solar stills with different methods of creating turbulence to enhance solar stills productivity in an effort to offer a full picture of current scientific advancements. These methods serve to induce turbulence in basin water and break the thermal boundary layer between still surface and water to enhance the evaporation. The use of turbulence devices converts free evaporation to forced evaporation, which increases the evaporation rate. Spraying unit, air bubbles, vibratory harmonic effect, stirring turbulence, rotating parts and ultrasonic fogger were used to create water turbulence. Diverse results (productivity and enhancement) demonstrated shown the importance of spraying unit (5400 mL/m2/day −56%), air bubbles (5490 mL/m2/day–21.96%), stirring turbulence (5400 mL/m2/day −39.49%), and ultrasonic fogger (6270 mL/m2/day– 83.87%). The benefit of this review is that it will allow for a systematic understanding of the role and influence of each thermal-methods on the daily productivity rate using various turbulence techniques.

Samimi, M., & Moghadam, H. (2024) [15] studied about the solar still, in which saline or brackish water is converted into freshwater using renewable solar energy, can be an effective solution to water scarcity. Inclined solar stills are well-known due to their high production yields compared to other types of solar stills. In this study, an inclined weir-type solar still was developed as a modified inclined solar still with an emphasis on the effect of structural parameters, such as weir height, distance between weirs, and distance between the absorber plate and the condenser cover, on distilled water production. The optimal values of structural parameters for the maximum freshwater production were specified by the response surface methodology and a quadratic model derived from a Box-Behnken design model. The results showed that the operational variables of the inclined weir-type solar still system significantly impacted the water production volume. Using a weir height of 2 cm, a distance of 3.5 cm between weirs, and a distance of 15 cm between the absorber plate and the condenser cover, the maximum water production volume was achieved at 6.474 kg m−2.day−1. The selected model had R^2, R_adj^2 and R_pred^2 values of 0.9978, 0.9939, and 0.9756, respectively. The maximum and minimum volumes of the produced water were obtained as 6.64125 and 1.79792 kg m−2. day1, based on the multiple response prediction of the variables. According to the validation tests, the model's accuracy in prediction of the maximum amount of freshwater production was notable (97.49%).

Aftiss, R. et al. (2024) [16] provided a detailed comparison of three types of solar stills: the conventional passive solar still (still-I), the solar still with paraffin wax as a phase change material (PCM) (still-II) and the solar still with PCM coupled to a storage tank (still-III). The study involves a numerical investigation across six regions of Morocco during typical days of each season of the year. The paper formulates and solves the thermal energy balance equations for the different components of the solar stills and storage tank. The numerical simulation is validated by comparing the results with existing experimental and numerical data. The study shows that a portion of the energy produced during the day is stored in the PCM, which can be utilized at night. In addition, the storage tank plays an active role in improving the yield of the passive solar still, indicating the advantage of the new configuration. Thus, the productivity of still-III during

typical days of spring, summer and autumn exceeds that of still-II and still-I. The maximum value of still-III was obtained in region five of Morocco (Marrakech) in spring with 8.6 kg.

Elamy, M. et al. (2024) [17] explored methods to enhance the performance of a coiled solar still (COSS), investigating various techniques to improve its efficiency and effectiveness in water purification. One technique involved adding a vertical wick distiller (VWSS) with built-in reflectors positioned after the COSS. Additionally, the research examined the impact of incorporating a fan and a separate condenser on the COSS's distillate output. Finally, the investigation assessed the potential advantages of incorporating paraffin wax infused with nanomaterial beneath the COSS base. The key findings revealed significant improvements in distillate production with the COSS modifications. Compared to a standard solar still (CSS), the COSS alone demonstrated a 76 % increase in daily output. Integrating a heating coil and internal reflectors with the COSS further boosted productivity by an impressive 92 %. The most significant advancements were achieved by combining the COSS with a VWSS and additional features. The MCOSS (COSS with VWSS and internal reflectors) exhibited a remarkable 209 % increase in distillate production compared to the CSS. This value increased to a staggering 269 % when incorporating a heating coil, VWSS, and an external condenser. Adding a fan to the MCOSS further enhanced efficiency to 68 %. Notably, incorporating nanomaterial-infused paraffin wax (PCM-Ag) with the MCOSS with VWSS resulted in a 246 % increase in productivity compared to the standard design. The research also revealed a significant decrease in freshwater production costs. The cost per liter of freshwater was determined to be $0.024 for the CSS and a considerably lower $0.0126 for the MCOSS with a fan.

Dubey, A., & Arora, A. (2024) [18] addressed the critical issue of potable water shortages faced by isolated communities in certain countries, highlighting the urgency of finding effective solutions to ensure access to clean water in these regions. Utilizing solar still (SS) has proven to be an effective and economical method for producing potable water, but it suffers from low productivity. Among the multiple innovative techniques employed to enhance the performance, employing phase change materials (PCMs) ensures enhanced incessant production of potable water during the night, thus bridging the gap between supply and demand. Further, as an emerging field, the application of nano-enhanced PCMs (NePCMs) has been found promising in augmenting the thermal conductivity of PCMs. In this manuscript, a review of the recent studies on the performance enhancement of solar stills incorporated with PCMs, nano-enhanced PCMs, hybrid PCMs, bioactive PCMs, etc., has been carried out. The novel approaches have demonstrated the enhancement of yield in the range of 31–100 % and 49.5–132 % by incorporating PCMs and NePCMs, respectively, using passive solar stills, while reaching a maximum of ∼140 % and ∼ 244 % with active solar stills. Bioactive NePCM has shown enhanced yield by ∼124.2 % compared to conventional solar still. The use of hybrid PCMs and NePCMs is found attractive and enhances the yield further by ∼9 % compared to single PCM. It is further revealed that adding sensible heat storage materials with basin water as a hybrid approach with PCMs/NePCMs loaded solar stills is promising, along with augmenting the performance using magnetic field and UV plasmon resonance. This review also emphasizes the opportunity and future research and would form a road map for the researchers to explore appropriate hybrid combinations to compete with the other technologies.

Essa, F. et al. (2024) [19] investigated a different mechanism of solar distillation through conducting a modified conventional solar still with corrugated shaped absorber (MCSS-CSA). To expand the MCSS-CSA's evaporation area, a vertical wick (VW) is added to the back and side walls. More other modifications such as integrating the MCSS-CSA-VW with a vertically positioned wick distiller (VWSS) and utilizing silver nanoparticles enhanced phase change material (PCM-Ag Nano). The location of the experiment was Kafrelsheikh, Egypt (31.1107° N, 30.9388° E). The experimental results demonstrated that the best thermal efficacy of 61.3 % was found for the MCSS-CSA-VW-PCM-Ag and VWSS configuration. In addition, the yield of MCSS-CSA-VW-PCM-Ag + VWSS was improved by 277 % over that of the CSS, where the total accumulation of productivity for MCSS-CSA-VW-PCM-Ag + VWSS and conventional distiller (CSS) was 11,700 and 3100 ml/m2, respectively. Moreover, the cost of desalinated water was 0.024 & 0.011 $/L for CSS and MCSS-CSA-VW-PCM-Ag + VWSS, severally.

Sathyamurthy, R. et al. (2024) [20] highlighted that, despite technical advancements, the critical need for fresh water remains unmet in many remote regions. This research investigates a solution by enhancing a single slope solar still (SSSS) with paraffin wax as an energy storage medium in recycled soda cans. These cans were coated with a unique mixture of black paint and carbon soot nanoparticles gathered from automobile engine exhausts to boost thermal conductivity and heat absorption. These nanoparticles, averaging 50–60 nm in size, greatly enhanced the heat absorption efficiency of the cans. Morphological examination demonstrated a consistent distribution of nanoparticles across the surfaces of the cans. The experimental setup was kept at a constant water depth in three different configurations: SSSS without phase change material (PCM) cans, SSSS with uncoated PCM cans, and SSSS with coated PCM cans. The SSSS with coated PCM cans showed significant improvements in thermal performance and cumulative yield, with gains of around 75.7 % and 102.3 %, respectively, when compared to the SSSS with uncoated PCM cans and those without energy storage. These findings show the potential for better waste management and renewable energy usage in delivering readily available drinkable water.

III. Objective

- To expand the productivity of solar still by varying geometrical parameters
- To optimize the mass flow of solar still
- Compare the conventional results by new proposed design of solar still
- To analyze the temperature, mass flow and to optimize the efficiency of solar still
- By compare all parameter solar still to validate the analytical from the conventional design

IV. Methodology

A. Design for a Solar Still

A solar still generates fresh water by harnessing solar energy. It features a slanted glass roof that lets in short-wavelength solar radiation while trapping longer-wavelength heat due to the greenhouse effect. This setup heats the still, causing evaporation and condensation of water. The roof absorbs and reflects some of the sunlight, with the glass walls also allowing short-wavelength radiation to enter, while longer-wavelength radiation is trapped inside.

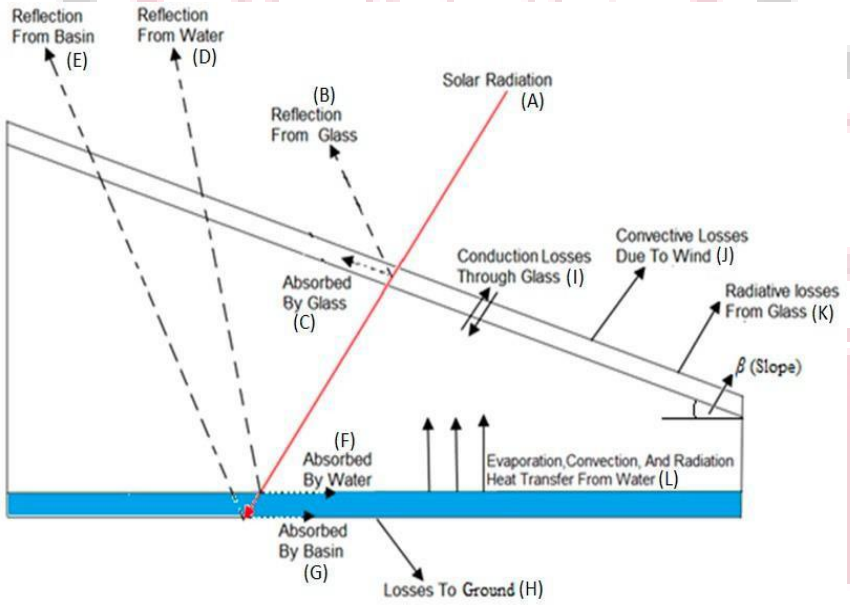

Figure 3 Work description of SS-Solar Still

In a solar still, brackish water absorbs solar energy, causing it to evaporate. Some energy is lost through reflection, conduction, and radiative and convective losses. The evaporated pure water condenses on the warmer inner glass surface and collects as fresh water. The remaining brackish water is drained and replaced.

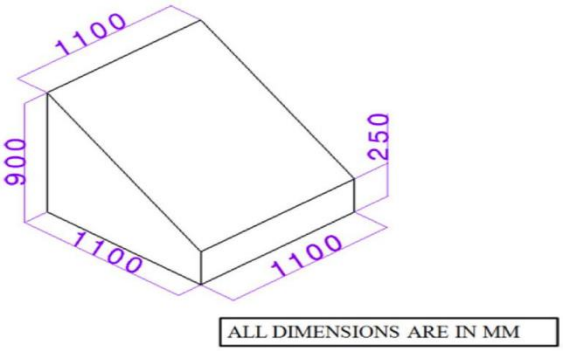

Figure 4 Geometry of single slope solar still

B. Productivity and thermal efficiency

Every experimental hour, the productivity of potable water was recorded in the current study. A solar still's daily productivity is calculated from how much fresh water cumulates in each day's working hours (d.w.h)

$$P_d = \sum_1^{d.w.?} \quad P_?$$ (4.1)

This is an evaluation of solar stills' fresh water productivity enhancement (penh.):

$$P_{en?} = \frac{(P_d)_m; (P_d)c}{(P_d)c} \times 100\% \quad (4.2)$$

Modified solar still $((P_d)_m)$ and conventional solar still $((P_d)c)$ produce freshwater at different levels

In solar stills, thermal efficiency is determined by comparing evaporation-condensation heat transfer per unit mass (q_e) with incident solar radiation (I).

$$\eta = \frac{q_e}{I} \times 100 = ?_{emq} \frac{(T_w; T_i)}{I} \times 100\% \quad (4.3)$$

The hourly productivity of fresh water in (kg/h) is defined as follows:

$$Ph = \frac{?_{ewg} A_b (T_w; T_i)}{L} \times 100\% \quad (4.4)$$

As a result, solar stills have the following hourly thermal efficiency:

$$\eta = \frac{P_h \times L}{A_g \times I \times 3600} \times 100\% \quad (4.5)$$

Hence, solar stills are calculated based on their thermal efficiency:

$$\eta_t = \frac{P_d \times L_{av}}{A_g \times \sum_1^{d.w.h} I \times 3600} \times 100\% \quad (4.6)$$

L is calculated in J/kg as follows or using online tables L is calculated based on ref.

The value of L is $(2503.3\text{-}2.398) \times T_w \times 103$ (4.7)

C. Parameters and Levels

The Taguchi technique, created by Genichi Taguchi, optimizes processes by minimizing variance and improving performance through a structured approach. It involves identifying parameters, setting their levels, designing experiments with an orthogonal array, choosing a performance measure, conducting and recording experiments, analyzing data, and finding optimal settings. For instance, a study by Ali et al. (2023) varied glass thickness (0.01-0.02 mm) and slope (20°-30°) in nine simulations based on the L9 array to assess mass flow rate under different sun intensities and angles.

Table 1 Parameter and Range

	I	II	III
Slope	20°	25°	30°
Glass thickness	0.01	0.02	0.03

Table 2 L9 Orthogonal Array

Run	Slope	Glass thickness, m
1	20°	0.01
2	25°	0.02
3	30°	0.03
4	20°	0.02
5	25°	0.03
6	30°	0.02
7	20°	0.03
8	25°	0.01
9	30°	0.02

D. Computational Fluid Dynamics Analysis of Solar Still

Computational Fluid Dynamics (CFD) analyzes fluid flow and heat transfer using simulations. This study uses ANSYS Fluent to model phase-shifting materials in solar stills, focusing on momentum and energy conservation. CFD software relies on three components: the pre-processor, solver, and post-processor.

Pre-Processor

As we advance with our analysis, our focus will shift to a comprehensive evaluation of the results, including examining domain geometry and grid displays, and creating line and shaded contour plots, as well as 2D and 3D surface plots. We will also explore colour Post Script output, vector plotting, and contour illustrations. Additionally, animation capabilities are now available for presenting variable outcomes, and all codes ensure reliable alpha-numeric results and data export options.

Solver

In computational fluid dynamics (CFD), methods like finite differences, finite elements, and spectral approaches are used, with finite volume methods being prominent in tools like CFX/ANSYS and FLUENT. This method involves integrating fluid equations across control volumes, discretizing them into algebraic equations, and solving iteratively. It uniquely focuses on ensuring the conservation of flow variables within each control volume, balancing increases and decreases in properties like velocity or enthalpy.

Post-Processor

In our analysis, we examine results using domain geometry, contour plots, surface plots, color outputs, and vector plots. We also utilize animations for variable outcomes and ensure reliable alpha-numeric results and data export capabilities.

Algorithm used for Computational Fluid Dynamics Analysis:

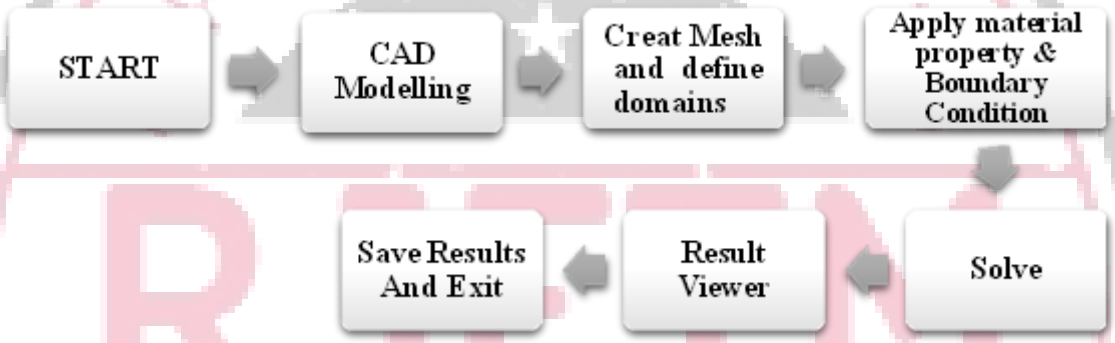

Figure 5 Algorithm used for CFD analysis

Governing Equations

The equation for conservation of mass, also known as the continuity equation, can be expressed in the following manner:

Conservation of Mass or Continuity Equation:

The equation for conservation of mass, also known as the continuity equation, can be expressed in the following manner:

$$\frac{\partial_\rho}{\partial_t} + \nabla \cdot \left(\rho \vec{v}\right) = S_m \quad (4.8)$$

Where $S_m =$ to promote fluidity and involvement: The continuous phase can accept additional mass or input from customizable sources.

In the case of 2D axisymmetric shapes, the continuity equation is expressed as:

$$\frac{\partial_\rho}{\partial_t} + \frac{\partial_{(\rho v_x)}}{\partial_x} \frac{\partial_{(\rho v_r)}}{\partial_r} + \frac{(\rho v_r)}{r} = S_m \quad (4.9)$$

When considering the values of axial and radial coordinates (x and r, respectively) alongside the respective velocities ($vx$and vr), an accurate representation of the given scenario arises

Equations for Conserving Momentum

The concept of conservation of momentum within an inertial reference frame can be described as follows:

$$\frac{\partial}{\partial_t}(\rho \vec{v}) + \nabla \cdot (\rho \vec{v} \vec{v}) = -\nabla p + \nabla \cdot (\bar{\bar{\tau}}) + \rho \vec{g} + \vec{F} \quad (4.10)$$

In which p equals static pressure?

$\bar{\bar{\tau}} =$ Atensor representing stress,

$\rho g^{\rightarrow}$= Weight of the body and gravitational force

$F^{\rightarrow}$ = Forces exerted by the external body

Intensity of stress $\bar{\tau}$ is specified by

$$\bar{\bar{\tau}} = \mu\left[\left(\nabla\vec{v} + \nabla\overrightarrow{v^T}\right) - \frac{2}{3}\nabla\cdot\vec{v}I\right] \quad (4.11)$$

Where μ = molecular viscosity

In this case, I equal the unit tensor,

Two-dimensional axisymmetric geometry is described by the following equations for momentum conservation:

$$\frac{\partial}{\partial_x}(\rho v\rho_x) + \frac{1}{r}\frac{\partial}{\partial_x}(rpv_xv_x) + \frac{1}{r}\frac{\partial}{\partial_r}(rpv_rv_r) - \frac{-\partial_\rho}{\partial_x}\frac{1}{r}\frac{\partial}{\partial_x}\left[r\mu\left(2\frac{\partial v_x}{v_x} - \frac{2}{3}(\nabla\cdot\vec{v})\right)\right] + \frac{1}{r}\frac{\partial}{\partial_r}\left[r\mu\left(\frac{\partial v_x}{\partial_r} + \frac{\partial v_r}{\partial_x}\right)\right] + \partial_x \quad (4.12)$$

And

$$\frac{\partial}{\partial_t}(\rho v_r) + \frac{1}{r}\frac{\partial}{\partial_x}(rpv_xv_r) + \frac{1}{r}\frac{\partial}{\partial_r}(rpv_rv_r) = -\frac{\partial_p}{\partial_r} + \frac{1}{r}\frac{\partial}{\partial_x}\left[r\mu\left(\frac{\partial v_r}{\partial_x} + \frac{\partial vx}{\partial_r}\right)\right] + \frac{1}{r}\frac{\partial}{\partial_r}\left[r\mu\left(2\frac{\partial v_r}{\partial_r} - \frac{2}{3}(\nabla\vec{v})\right)\right] - 2\mu\frac{v_r}{r^2} + \frac{2\mu}{3r}(\nabla\cdot\vec{v}) + \rho\frac{n_z^2}{r} + F_r \quad (4.13)$$

Where,

$$\nabla\cdot\vec{v} = \frac{\partial v_x}{\partial_x} + \frac{\partial v_r}{\partial_r} + \frac{v_r}{r} \quad (4.14)$$

Where

v_x = Velocity along the axis

v_r=Intensity ofradiation

$\boldsymbol{v_z}$=Velocityoftheswirl

Formula for Calculating Energy

$$\frac{\partial}{\partial_t}\sum n_{K<1}(\alpha_K\rho_KE_K) + \nabla\cdot\sum n_{K<1}\left(\alpha_K\vec{v}_K(\rho_KE_K + p)\right) = \nabla\cdot\left(K_{eff}\,\nabla T\right) + S_E \quad (4.15)$$

Wherek_{eff}=Conductivityofeffectivematerials

S_E= Heating sourcesbasedonvolume

$$E_K = h_K - \frac{p}{\rho_k} + \frac{k^2}{2} \quad (4.16)$$

Where

$E_K = h_K$ for a phase of incompressibility and h_K= sensitive enthalpy for phase k

k−∈Model

By solving the following transport equations, we can obtain turbulence's kinetic energy, k, and its corresponding rate of dissipation,

$$\frac{\partial}{\partial_t}(\rho k) + \frac{\partial}{\partial x_i}\left(\rho_{\mathrm{kv}_i}\right) = \frac{\partial}{\partial x_j}\left[\left(\mu\frac{\mu_t}{\sigma_k}\right)\frac{\partial_k}{\partial x_j}\right] + G_k + G_b - \in -\gamma_M + S_k \quad (4.17)$$

And

$$\frac{\partial}{\partial_t}(\rho\in) + \frac{\partial}{\partial x_i}(\rho\in v_i) = \frac{\partial}{\partial x_j}\left[\left(\mu\frac{\mu_t}{\sigma_\in}\right)\frac{\partial_\in}{\partial x_j}\right] C_{1\in}\frac{\in}{k}(G_k + C_{3\in}G_b) - C_{2\in}\rho\frac{\in^2}{k} + s_\in \quad (4.18)$$

Asaresultofthemeanvelocitygradientsoftheseequations,turbulencekineticenergyis generated.

G_b As turbulence is produced by buoyancy, it produces kinetic energy

Y_M There is an integral contribution to the overall dissipation rate from oscillating dilatation in compressible turbulence.

$C_{1\in}$, $C_{2\in}$, and $C_{3\in}$ they remain constant.

$\sigma_k$and$\sigma_\in$ The Prandtl numbers for k are known to be turbulent ∈,

S_k and $S_\epsilon$the user can define their own source terms easily and engagingly.

CFD Analysis

1. CAD Model of a Single Slope Solar Still

Three-dimensional CAD models have been created using ANSYS design modular to demonstrate a single slope solar still in detail. In addition to the base measurements of 1.1 m by 1.1 m, the front and back walls have dimensions of 0.25 m and 0.9 m, respectively. Refer to figure 6 for a visual representation of the three-dimensional CAD model of the solar still.

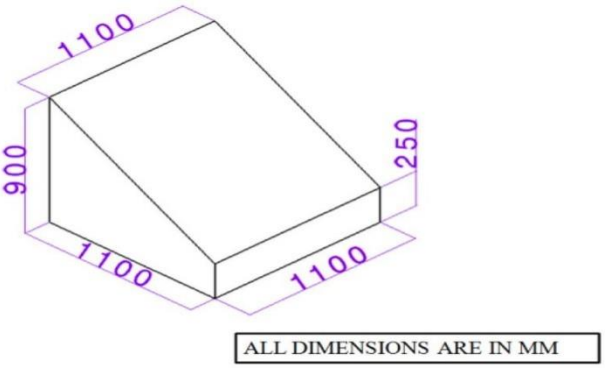

Figure 6 CAD model of single slope solar still

Meshing

After completing the CAD geometry of the single slope solar still, it was imported into ANSYS Workbench for analysis. The next step was meshing, where the geometry was divided into small elements for finite element analysis. Figure 7 illustrates this process, showing a mesh with 137,082 nodes and 128,832 hexahedral elements.

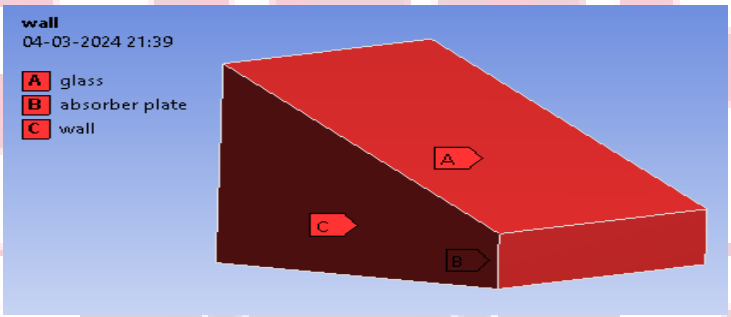

Figure 7 Different boundaries of single slope solar still

2. SingleSlopeSolarStillModel using CAD

An extensively detailed 3D CAD model for a double-slope solar still was built utilizing ANSYS design modular, computing the measurement of the base at 2.2 m x 1.1 whereas the front wall stands at 0.25 m, while the back wall computes 0.9. m. Have a look at figure 8 for a visual representation of the solar still's three-dimensional CAD model.

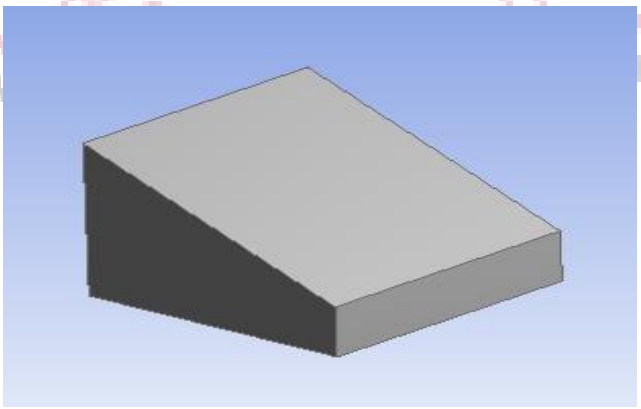

Figure 8 CAD model of double slope solar still with slope angle 25o

Meshing

When the CAD geometry of the double slope solar still is finalized, for additional analysis the next step involves introducing ANSYS workbench. Subsequently, the meshing process was carried out. The resulting mesh for the double slope solar still is illustrated in figure 9. A total of 446550 nodes and 427794 elements were generated using hexahedral elements.

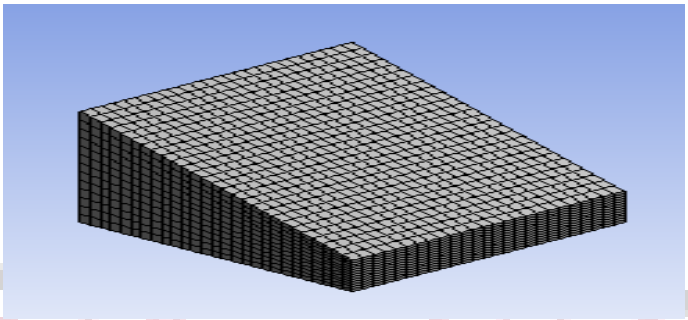

Figure 9 Meshing of single slope solar still through 25°

Material properties

In table 3, the thermo-physical properties of paraffin C18 material is mentioned which is used as PCM. In Tables thermo-physical properties of Glass, Steel and Wood are mentioned, which were obtained from ANSYS CFD software itself.

Table 3 Thermo-physical property of paraffin C18 material.

Property	Value
LatentHeatofFusion	245 KJ/Kg
MeltingPoint	301K
Thermalconductivity	0.148W/m-K
Density	865 Kg/m^3

Table 4 Thermo-physical property of glass

Property	Value
SpecificHeat	750J/Kg-K
Thermal conductivity	1.15 W/m-K
Density	2500 Kg/m3

Table 5 Thermo-physical property of steel

Property	Value
SpecificHeat	502.48J/Kg-K
Density	8030 Kg/m^3
Thermalconductivity	16.27W/m-K

Table 6 Thermo-physical property of wood

Property	Value
Thermalconductivity	0.173 W/m-K
Specific Heat	2310 J/Kg-k

Density	700 Kg/m³

Boundary conditions

Table 10 Boundary Conditions

Boundary Name	**Absorber plate**	**Front wall**	**Backwall**	**Glass**	**Side wall(left)**	**Side wall (right)**
Type	Wall	Wall	Wall	Wall	Wall	Wall
Thermal conditions	Adiabatic wall(Heat flux = 0)	Adiabatic wall(Heat flux = 0) (Heatflux = 0)	Adiabatic wall(Heat flux = 0)	Constant Heatflux (1000 W/m²)	Adiabatic wall (Heatflux = 0)	Adiabatic wall (Heatflux = 0)
Body type	Opaque	Opaque	Opaque	Semi-transparent	Opaque	Opaque

Table 11 CFD Analysis Input parameters

Setup		**Descriptions**
General	General	Absolutevelocityformulation,pressurebasedsteadystate analysis. Gravity=-9.81m/s² iny-direction
Model	Multiphase	Volume of fluid, Implicitformulation, SharpInterfacemodelling NumberofEulerian phase=3
	Energy	On
	Viscous	K-epsilon,StandardmodelwithStandardwallfunction
	Radiation	RosselandRadiationModel, Solar Ray Tracing method with Direct solar irradiation = 1000W/m²,Longitude77.4°E,Latitude23.2599°N,Time zone GMT+5:30 hour
Materials	Fluid	Air,Water-liquid,Water-vapour
	Solid	Glass,Steel,Wood
Phase	Primary	Air, Masstransfermechanism:evaporation-condensation
	Secondary-1	Water-liquid, Masstransfermechanism:evaporation-condensation
	Secondary-2	Water vapor, Masstransfermechanism:evaporation-condensation
Solution	Pressure-Velocitycoupling,Scheme-SIMPLE.	
	Spatial Discretization: Momentum-SecondorderUpwind, Volumefraction- Compressive, TurbulentKE&Dissipationrate-SecondorderUpwind, Energy- Second order Upwind	

V. Results and Discussion

This study aims to determine the maximum water production of a double sloped solar still (DS-Solar Still) and compare its efficiency to validate the study on CFD analysis of solar stills. The study used ANSYS to model and analyze both single and double sloped solar stills. The single slope model measured 110 cm x 110 cm with a 25 cm front wall and a 0.9 cm back wall. Results were compared to assess performance.

Table12 Comparisonofcurrentworkatdifferentfactors

S. No	Factors	C.Gnanaveletal (2020)	Currentwork	Percentage Difference
1	Water Volume Fraction on Glass	0.1056	0.1095	3.69%
2	Temperature (K)	305.1	311.2	1.99%

CFD Analysis of SS-Solar Still

After performing computational fluid dynamics (CFD) analysis on single slope solar still for mass flow of condense liquid following contour has been observed on a section in X-Y plane and at Z = 0.55 m, the maximum value of mass flow rate of 2.198e-2 kg/s-m2 as shown in figure 10.

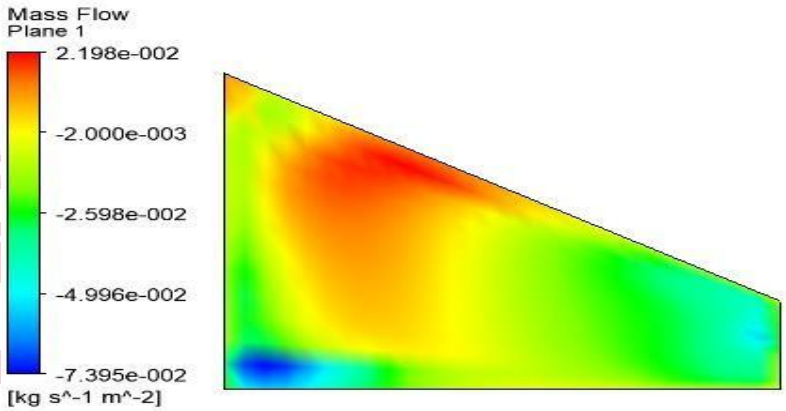

Figure 10 Contour result of mass flow in the solar still for model 1

Following computational fluid dynamics (CFD) analysis of a SS- Solar Still, an outline of the mass flow of condensed liquid has been observed on a section in the X-Y plane. At Z = 0.55 m, the maximum mass flow rate of 1.961e-2 kg/s-m² is depicted in figure 10.

Simulation Results

Table 13 Simulation Results-L9 orthogonal array

Run	Slope	Glassthickness,m	Mass flow rate, Kg/s-m2	Productivity, ml/hr
1	20°	0.01	0.0219	219.43
2	25°	0.02	0.0019	221.16
3	30°	0.03	0.2118	224.29
4	20°	0.02	0.0055	262.36
5	25°	0.03	0.0034	272.79
6	30°	0.02	0.029	291.22
7	20°	0.03	0.039	276.44
8	25°	0.01	0.0036	281.39
9	30°	0.02	0.0033	286.72

Table 13 shows the results of simulation run.

Calculation of productivity of single slope solar still:

The expression below is used for calculating how much output is produced in one hour.

$$P_h = \frac{h_{evap}(T_w - T_g) \times 3600}{\lambda} \quad (5.1)$$

h_{evap} =Evaporation heat transfer coefficient between the basin water and the glass

$$h_{evap} = 16.273 \times 10^{-3} \times h_c \times \left[\frac{P_w - P_g}{T_w - T_g}\right] \quad (5.2)$$

Where,

h_c = Convective heat transfer coefficient from basin water to glass cover

P_w = Vapour pressure of basin water

P_g = Vapour pressure of glass water

$$P = \exp\left[25.317 - \frac{5144}{T+273}\right] \quad (5.3)$$

T_w= Temperature of water (36.8°C) obtained from CFD simulation

$$T_g = \frac{T_{in} + T_{out}}{2} \quad (5.4)$$

Let T_{in}= 25 °C

$T_w = T_{out}$ = 36.8 °C

$$T_g = \frac{25 + 36.7}{2} = 30.85\ ^\circ\text{C}$$

$$P_w = \exp\left[25.317 - \frac{5144}{T_w + 273}\right]$$

$$P_w = \exp\left[25.317 - \frac{5144}{36.8 + 273}\right]$$

$$\boldsymbol{P_w = 6063.24\ Pa}$$

$$P_g = \exp\left[25.317 - \frac{5144}{T_g + 273}\right]$$

$$P_g = \exp\left[25.317 - \frac{5144}{32.9 + 273}\right]$$

$$\boldsymbol{P_g = 4914.76\ Pa}$$

$$h_c = 0.884\left[T_w - T_g + \left\{\frac{(P_w - P_g)(T_w + 273)}{268900 - P_w}\right\}\right]^{1/3}$$

$$h_c = 0.884\left[38.2 - 31.6 + \left\{\frac{(6063.24 - 4914.76)(36.8 + 273)}{268900 - 6063.24}\right\}\right]^{1/3}$$

$$h_c = 0.884\left[38.2 - 31.6 + \left\{\frac{(1148.48)(309.8)}{262836}\right\}\right]^{1/3}$$

$$h_c = 0.884[38.2 - 31.6 + \{1.353\}]^{1/3}$$

$$\boldsymbol{h_c = 6.841\ {}^{W}/_{m^2.K}}$$

$$h_{evap} = 16.273 \times 10^{-3} \times h_c \times \left[\frac{P_w - P_g}{T_w - T_g}\right]$$

$$h_{evap} = 16.273 \times 10^{-3} \times 6.841 \times \left[\frac{6063.24 - 4914.76}{36.8 - 32.9}\right]$$

$$h_{evap} = 16.273 \times 10^{-3} \times 6.841 \times \left[\frac{1148.48}{3.9}\right]$$

$$\boldsymbol{h_{evap} = 32.77\ {}^{W}/_{m^2.K}}$$

λ = Latent heat of vaporization of water during the day 2410.29 [kJ/kg]

$$P_h = \frac{h_{evap}(T_w - T_g) \times 3600}{\lambda}$$

$$P_h = \frac{32.77\ (36.8 - 30.85) \times 3600}{2410.29}$$

$$\boldsymbol{P_h = 291.22\ ml/hr}$$

Optimisation

Table 14 shows the response table for vapour density.

Table 14 Response Table for Signal to Noise Ratios for mass flow

Level	Slope	Glass thickness, m
1	0.0785	0.0221
2	0.0126	0.0029
3	0.0153	0.0813
Delta	0.0659	0.0784
Rank	2	1

For each level of these factors, we have corresponding values of 0.0221, 0.0029, and 0.0813 for glass thickness; 0.0785, 0.0126, and 0.0153 for slope. The delta values represent the differences between the maximum and minimum values for each factor. In this case, the delta for slope is 0.0659, and the delta for glass thickness is 0.0784. The rank indicates the relative importance of each factor. In this case, for the factor "Slope," it has the smallest delta (0.0659), and thus, it has been assigned a rank of 2. For the factor "Glass thickness," it has a larger delta (0.0784), and it has been assigned a rank of 1.

Table 15 Response Table for Signal to Noise Ratios for productivity

Level	Slope	Glass thickness, m
1	46.91	48.01
2	48.79	48.20
3	48.99	48.48
Delta	2.08	0.47
Rank	1	2

Results Confirmation

Table 16 Parameter determination and comparison

Parameter	Conventional solar still	Optimized solar still
A1B3	0.0332	0.039 Kg/s-m^2
A3B3	221.67	224.24 ml/hr

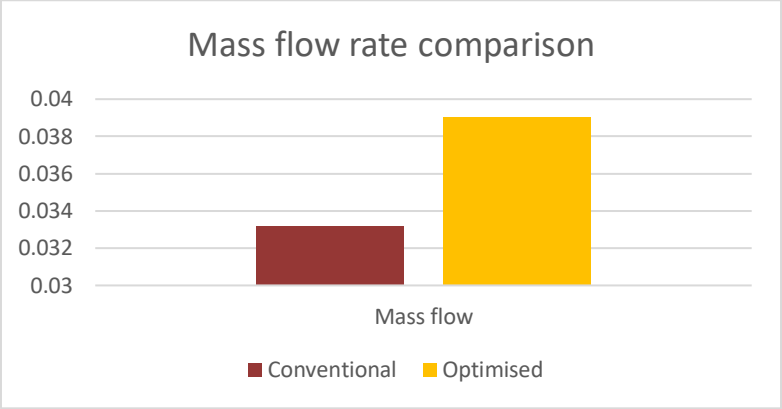

Figure 11 Mass flow rate comparison

VI. CONCLUSION

This study successfully optimized solar stills to significantly enhance potable water production, addressing the pressing global need for clean drinking water. The study utilized ANSYS simulations to compare the performance of single and double sloped solar still designs, revealing notable improvements in water yield through various turbulence-enhancing methods. Among these, ultrasonic fogging was particularly effective, achieving up to an 83.87% increase in productivity. In addition to exploring turbulence techniques, the study focused on optimizing structural parameters of inclined solar stills, such as adjusting weir height and the distance between key components. These optimizations led to a maximum water production rate of 6.474 kg/m² per day. The findings highlight the substantial potential for improving the efficiency of solar distillation systems through thoughtful design modifications and innovative turbulence methods. These advancements not only provide valuable insights into enhancing solar still performance but also offer practical solutions for addressing the global challenge of water scarcity. By validating the effectiveness of the proposed design modifications, this study underscores their relevance in advancing sustainable and efficient water purification technologies.

References

[1] El-Sebaii, A. A., Al-Ghamdi, A. A., Al-Hazmi, F. S., & Faidah, A. S. (2009). Thermal performance of a single basin solar still with PCM as a storage medium. Applied Energy, 86(7-8), 1187-1195. https://doi.org/10.1016/j.apenergy.2008.10.014

[2] Kabeel, A. E., & Abdelgaied, M. (2016). Improving the performance of solar still by using PCM as a thermal storage medium under Egyptian conditions. Desalination, 383, 22-28. https://doi.org/10.1016/j.desal.2016.01.006

[3] Al-harahsheh, M., Abu-Arabi, M., Mousa, H., & Alzghoul, Z. (2018). Solar desalination using solar still enhanced by external solar collector and PCM. Applied Thermal Engineering, 128, 1030-1040. https://doi.org/10.1016/j.applthermaleng.2017.09.073

[4] Sonker, Varun & Chakraborty, Jyoti & Sarkar, A. & Singh, Rishikesh. (2019). Solar distillation using three different phase change materials stored in a copper cylinder. Energy Reports. 5. 1532-1542. 10.1016/j.egyr.2019.10.023.

[5] Shalaby, S. M., El-Bialy, E., & El-Sebaii, A. A. (2016). An experimental investigation of a v-corrugated absorber single-basin solar still using PCM. Desalination, 398, 247-255. https://doi.org/10.1016/j.desal.2016.07.042

[6] Shinde, M., Navthar, R., & Shinde, S. M. (2022). Review on the types of solar stills. International Journal of Ambient Energy, 43(1), 1420-1428. https://doi.org/10.1080/01430750.2019.1707114

[7] Yang, T., King, W. P., & Miljkovic, N. (2021). Phase change material-based thermal energy storage. Cell Reports Physical Science, 2(8). https://doi.org/10.1016/j.xcrp.2021.100540

[8] Samykano, M. (2022). Role of phase change materials in thermal energy storage: Potential, recent progress and technical challenges. Sustainable Energy Technologies and Assessments, 52, 102234. https://doi.org/10.1016/j.seta.2022.102234

[9] Hemmatian, A., Kargarsharifabad, H., Esfahlani, A. A., Rahbar, N., & Shoeibi, S. (2024). Improving solar still performance with heat pipe/pulsating heat pipe evacuated tube solar collectors and PCM: An experimental and environmental analysis. Solar Energy, 269, 112371. https://doi.org/10.1016/j.solener.2024.112371

[10] Almeshaal, M., & Shanmugan, S. (2024). Improving thermal efficiency of solar stills: Bioactive nano-PCM and Cramer's rule analysis. Separation and Purification Technology, 343, 127119. https://doi.org/10.1016/j.seppur.2024.127119

[11] Alsaman, A. S., Maher, H., Ghazy, M., Ali, E. S., Askalany, A. A., & Saha, B. B. (2024). 2D materials for adsorption desalination applications: A state of the art. Thermal Science and Engineering Progress, 102455. https://doi.org/10.1016/j.tsep.2024.102455

[12] García-Ávila, F., Guanoquiza-Suárez, M., Guzmán-Galarza, J., Cabello-Torres, R., & Valdiviezo-Gonzales, L. (2023). Rainwater harvesting and storage systems for domestic supply: An overview of research for water scarcity management in rural areas. Results in engineering, 18, 101153. https://doi.org/10.1016/j.rineng.2023.101153

[13] Lillo-Bravo, I., Vera-Medina, J., Fernandez-Peruchena, C., Perez-Aparicio, E., Lopez-Alvarez, J. A., & Delgado-Sanchez, J. M. (2023). Random Forest model to predict solar water heating system performance. Renewable Energy, 216, 119086. https://doi.org/10.1016/j.renene.2023.119086

[14] Abdullah, A. S., Panchal, H., Alawee, W. H., & Omara, Z. M. (2023). Methods used to improve solar still performance with generated turbulence for water desalination-detailed review. Results in Engineering, 101251. https://doi.org/10.1016/j.rineng.2023.101251

[15] Samimi, M., & Moghadam, H. (2024). Investigation of structural parameters for inclined weir-type solar stills. Renewable and Sustainable Energy Reviews, 190, 113969. https://doi.org/10.1016/j.rser.2023.113969

[16] Aftiss, R., Najim, M., & Hissouf, M. (2024). Numerical study of PCM-integrated solar still efficiency enhancement. International Journal of Low-Carbon Technologies, 19, 443-454. https://doi.org/10.1093/ijlct/ctae004

[17] Elamy, M. I., Mohammed, S. A., Basem, A., Alawee, W. H., Abdullah, A. S., Aldabesh, A., ... & Essa, F. A. (2024). Enhancing coiled solar still performance with vertical wick distiller, reflectors, nanomaterial-infused PCM, and condenser integration. Case Studies in Thermal Engineering, 61, 104912. https://doi.org/10.1016/j.csite.2024.104912

[18] Dubey, A., & Arora, A. (2024). Effect of various energy storage phase change materials (PCMs) and nano-enhanced PCMs on the performance of solar stills: A review. Journal of Energy Storage, 97, 112938. https://doi.org/10.1016/j.est.2024.112938

[19] Essa, F. A., Eldesoukey, A., Baz, F. B., Omara, Z. M., & Amro, M. I. (2024). Enhancing solar still thermal performance through synergistic effects of silver nanomaterial-enhanced phase change material and geometric modifications. Journal of Energy Storage, 98, 113168. https://doi.org/10.1016/j.est.2024.113168

[20] Sathyamurthy, R., Ali, H. M., Said, Z., El-Sebaey, M. S., Gopalsamy, S., Nagaraj, M., ... & Alomar, T. S. (2024). Enhancing solar still thermal performance: The role of surface coating and thermal energy storage in repurposed soda cans. Journal of Energy Storage, 77, 109807.